Structure of Liquid *N*-Methylacetamide: Temperature Dependence of NMR Chemical Shifts and Quadrupole Coupling Constants

R. Ludwig*

Physikalische Chemie, Fachbereich Chemie der Universität Dortmund, 44221 Dortmund, Germany

F. Weinhold and T. C. Farrar

Theoretical Chemistry Institute and Department of Chemistry, University of Wisconsin—Madison, Madison, Wisconsin 53706

Received: April 21, 1997; In Final Form: August 27, 1997[⊗]

Temperature-dependent NMR chemical shifts and quadrupole coupling constants for the amide hydrogen, the nitrogen, and the carbonyl oxygen nuclei in neat, liquid *N*-methylacetamide are calculated by ab initio methods and compared with experimental measurements. These calculations are based on ab initio quantum cluster equilibrium (QCE) theory and standard ab initio self-consistent-field (SCF) methods at the 3-21G and 6-31G* levels for five different molecular clusters. The cluster sizes varied from the monomer up to a five-membered linear structure of *N*-methylacetamide. Strong cooperative effects are found in the molecular clusters and are reflected in the geometries, chemical shifts, and quadrupole coupling values for each species. The equilibrium populations of the clusters were calculated between the melting (301 K) and the boiling point (478 K). At low temperatures the linear pentamer is the dominant species. At higher temperatures these clusters are replaced by linear dimers and monomers. The calculated chemical shift values for the ^{1}H, ^{17}O, the ^{14}N nuclei are in excellent agreement with experimental NMR data. The calculated quadrupole coupling constants for the amide deuteron and the nitrogen nucleus likewise agree well with the temperature behavior found in NMR relaxation time experiments.

1. Introduction

N-Methylacetamide (NMA) is an important model system for proteins. Although it has been extensively studied both experimentally[1−26] and theoretically,[27−45] uncertainties still exist concerning the effect of hydrogen bonding on its structure and conformation. Protein hydrogen bonds involving the peptide backbone are essential for the existence of the native structure, but the importance of the hydrogen bonding to the protein stability is still unclear. Many studies have focused on the ability of water molecules to compete with peptide hydrogen bonds. Recent ab initio calculations[38,39] have shown that the solvent for a protein solution has a very significant effect on the strength of the protein hydrogen bonds. The cooperative stabilization effects are sufficiently large that they must be considered in any analysis of either the solvent denaturation or the enhancement of helix stability in peptides and proteins.[46−54] Karplus et al.[55] suggested that it may sometimes be necessary to introduce corrections to the pairwise-additive potentials used in molecular dynamics studies.

Sensitive experimental probes of liquid structure are provided by NMR chemical shifts, the quadrupole coupling constant (QCC), χ_Q, and its associated asymmetry parameter, η_Q (we denote a general quadrupole coupling constant by χ_Q and nitrogen, oxygen, and deuterium quadrupole coupling constants by χ_N, χ_O, and χ_D, respectively; a similar convention is used for the associated asymmetry parameters, η_N, η_O, and η_D). These NMR properties have long been recognized as being extremely sensitive to local electron distributions, bond hybridization states, proximity to polar groups, and local magnetic anisotropies; several empirical equations that relate chemical shifts[56] and quadrupole coupling constants[57−59] to molecular structure have been established.

The present work is focused on rigorous experimental NMR tests of a new theory for describing the equilibrium liquid properties of *N*-methylacetamide and other strongly H-bonded liquids: quantum cluster equilibrium (QCE) theory.[60] As its name implies, QCE theory is based on a full quantum treatment of the H-bonded clusters that are considered to be the fundamental constituent units of the neat liquid and gaseous (fluid) phases. The cluster equilibria that describe phase composition can be calculated by the rigorous techniques of quantum statistical thermodynamics in the canonical ensemble, based on the ab initio partition function for each cluster. For a given T and P solution of the cluster equilibrium conditions (equality of stoichiometrically weighted chemical potential for each cluster type) typically leads to several distinct roots (phases), each corresponding to distinct density and cluster populations. The QCE root of lowest Gibbs free energy corresponds to the equilibrium phase. The associated cluster population distribution then provides the proper weighting factors to compute the (T,P)-dependent equilibrium values of any spectroscopic parameters associated with the various clusters. Comparison of these theoretical values with experimental measurements provides a stringent test of the QCE population distributions and the associated (T,P)-dependent cluster picture of the equilibrium liquid structure.

Previous applications of the QCE method have led to a remarkable picture of the equilibrium liquid clusters in water[62] and formamide.[63,64] In both cases, large cyclic clusters (e.g., cyclic pentamers and hexamers) were found to dominate the neat liquid, with each monomer unit participating in exactly *two* H-bonds cooperatively arranged around the ring. In formamide, the dominant clusters under near-ambient conditions were found to be cyclic hexamers (95%) and linear tetramers (4%), leading to predicted QCC and anisotropy values that are in excellent agreement with those found experimentally. In

[⊗] Abstract published in *Advance ACS Abstracts,* November 1, 1997.

S1089-5639(97)01360-1 CCC: $14.00

water, in the experimentally accessible temperature region, the corresponding QCE population distributions were found to involve primarily cyclic octamers, leading to the prediction of negligible temperature variations of the oxygen and deuterium QCC values (η_O, and η_D), again in agreement with experiment.

A striking feature of the dominant QCE clusters for formamide is that H-bonding is found to involve only the N−H bond which is trans (anti) to the oxygen, with all carbonyl C−H bonds pointing inward toward the center of cluster. Methyl substitution is therefore expected to have a dramatic influence on the ringlike topology, depending on whether N-methyl or C-methyl derivatives are chosen. In the former case (*N*-methylformamide, treated in a previous paper), the methyl group replaces the cis amide proton which lies outside the hexagonal structure and is not hydrogen bonded. In this case one anticipates that methyl substitution would involve little or no disruption of ring topology. However, methyl substitution at the carbonyl proton (as in acetamide or NMA, the subject of the present work) creates severe steric congestion near the ring center, effectively preventing ring formation except in much larger cluster sizes that are disfavored on entropic grounds.

Since ring topologies are effectively "forbidden" for NMA, the QCE cluster distributions of liquid NMA are expected to differ dramatically from those found previously for formamide or NMF. This, in turn, leads to significantly different NMR chemical shift and quadrupole coupling parameters. The purpose of the present work is to calculate the NMR and NQR parameters based on the QCE model in order to test the predictions with experimental measurements over the entire liquid range (301−478 K). Available structural data from X-ray and neutron diffraction studies are also compared with the QCE predictions.

The emerging QCE picture of liquid structure complements conventional molecular dynamics (MD) simulation models based on pairwise-additive potential functions of classical electrostatic form and strongly suggests that more realistic potential functions are needed. The present work demonstrates the important role of supramolecular cooperative effects in stabilizing certain cluster geometries; in some NMA cases the average H-bond strength is enhanced by up to 40% relative to that of the dimer. These cooperative effects are therefore necessary for even a qualitatively correct picture of cluster energetics. In addition, the entropic properties (primarily vibrational in origin) of dominant QCE clusters are significantly altered by cooperative binding effects. A more detailed discussion of cluster vibrational properties of liquid NMA and comparison with spectroscopic IR measurements are presented in a forthcoming paper.[66]

2. Computational Method

Ab initio calculations were carried out at the uncorrelated, restricted Hartree−Fock (RHF) level for four stable conformers of the *trans-N*-methylacetamide (NMA) monomers that result from conformational isomerism of the CH_3 groups and for four larger NMA $(CH_3OCNHCH_3)_n$ clusters, $n = 2-5$. The five most important geometries are shown in Figure 1. To calculate the cluster populations, we used ab initio 3-21G optimized geometries, harmonic frequencies, and binding energies. These values were then used to calculate an ab initio partition function for each cluster using standard statistical thermodynamic methods. In the electronic partition function, ab initio RHF/3-21G binding energies are corrected with full counterpoise calculations[68] for the effects of basis set superposition errors. Residual cluster−cluster interactions are taken into account by a mean-field correction which is proportional to the system density.[60]

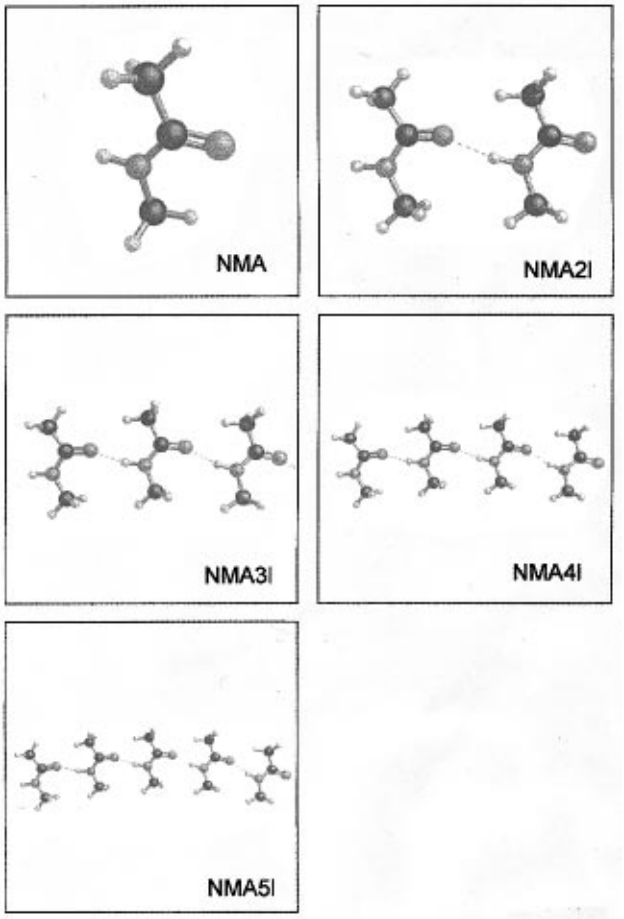

Figure 1. The five most important linear clusters for *N*-methylacetamide, $n = 1-5$.

Although qualitatively reasonable, the mean-field treatment is not entirely satisfactory. However, even complete neglect of this correction does not grossly affect equilibrium liquid populations and has practically no effect on gas-phase properties. The current treatment of molecular volume used in evaluating the translational partition function is also a concern. An overall proportionality factor (chosen to fix system density at a single point, the standard state) can be altered to ensure that gross populations are relatively insensitive to these volume estimates. The results for the cluster populations clearly depend on whether all significant clusters have been included in the mixture. Although we include here only the clusters with significant populations, many more, less significant cluster types were screened.

It may be noted that certain types of expected temperature dependence are ignored in this simplified treatment. We previously noted[62] that the thermodynamic behavior is quite insensitive to conformational equilibria that do not significantly alter average H-bond strength and directionality, so it is generally necessary to include only "representative" conformers of each topology class in the QCE cluster mixture. (Such an approximation would not be appropriate for properties that depend strongly on the neglected conformational isomerization.) One can also anticipate that the apparent cluster "volume" should be somewhat temperature-dependent, due to the (neglected) anharmonicity of thermally excited vibrational motions, as well as the finite "softness" of steric exchange potentials with respect to thermal collisions of varying ambient kinetic energy. Furthermore, the residual mean-field cluster−cluster interactions may exhibit slight temperature dependence (as, for example, in a Keesom potential[61]). The latter dependencies might be

incorporated in the QCE model by allowing volume and mean-field parameters to become temperature-dependent, but such refinements appear unnecessary in the present treatment.

The condition of chemical equilibrium is employed to find the cluster populations for the phase of lowest free energy at a specific temperature and pressure. In the present case, the stable liquid phase at standard-state conditions is calculated to lie 12.6 kJ/mol below the low-density vapor phase. Macroscopic properties such as isotropic chemical shifts (σ_{iso}), electric field gradients (efg), efg asymmetry parameters (η_Q), and molecular geometries are calculated by weighting the properties of each cluster by the appropriate cluster population. The σ_{iso}, efg, and η_Q values for the ^{1}H, ^{17}O, and ^{14}N nuclei in all clusters were calculated at the 6-31G* basis level, keeping the geometries of the clusters fixed at the values obtained at the 3-21G level.[69]

Chemical shielding calculations were performed using gauge-including atomic orbitals (GIAO) as implemented in Gaussian 94.[70] The isotropic chemical shielding is obtained by averaging the three principal tensor components of the chemical shielding tensor: σ_{xx}, σ_{yy}, and σ_{zz}. Quadrupolar coupling constants (QCC) and asymmetry parameters were calculated using QCC $= eq_{zz}$ eQ and $\eta = q_{xx} - q_{yy}/q_{zz}$, where eQ is the nuclear electric quadrupole moment of the nucleus, and q_{xx}, q_{yy}, and q_{zz} are the tensor components of the electric field gradient (efg) tensor.

3. Experimental Method

All compounds used in this work were obtained from Aldrich Chemical Co., Inc., and were used without further purification. The samples were degassed by several freeze−pump−thaw cycles. All experiments were performed on naturally abundant isotopic materials. The NMR chemical shift data for ^{1}H, ^{17}O, and ^{14}N were obtained with a Bruker AM-500 spectrometer operating at 500.13, 67.80, and 36.14 MHz, respectively. At 303 K the field homogeneity was optimized using dimethyl sulfoxide-d_6 (DMSO) and acetone-d_6. No field lock was used during data acquisition. The chemical shifts (ppm) were determined relative to internal references such as tetramethylsilane (TMS) for the amide proton and dimethyl sulfoxide (DMSO) for the carbonyl oxygen. For nitrogen no internal reference was used, because available reference compounds such as ammonium hydroxide solution depend strongly on temperature and on concentration. In this case the measurements were performed using an external reference and the temperature-dependent chemical shifts are referred to the values at the lowest temperature. The estimated errors for the chemical shifts are less than ±0.01 ppm for ^{1}H and less than ±0.20 ppm for ^{14}N and ^{17}O.

Chemical shifts were not corrected for bulk magnetic susceptibility effects. For the ^{17}O experiments the following data acquisition parameters were used: spectral width 50 kHz, 90° pulse 18 μs, quadrature phase detection, acquisition time $\sim 5T_2$. Typically, 5000 transients were recorded for each ^{17}O spectrum.

4. Results and Discussion

4.1. Cluster Structural, Energetic, and NMR Properties. The preferred conformation of the NMA monomer[31,44,45] is shown in Figure 1, with both methyl groups having an in-plane C−H bond oriented in proximity to the carbonyl C═O. The optimized RHF/3-21G geometry of this conformer is compared with experimental gas- and crystal-phase geometries in Table 1. From this monomeric form, higher NMA clusters up to the pentamer were similarly optimized at the RHF/3-21G level and tested for stability with harmonic frequency analysis. As shown in Figure 1 (and used in all the tables), we employ the labels NMA, NMA2l, NMA3l, NMA4l, and NMA5l for linear dimer, trimer, tetramer, and pentamer, respectively.

TABLE 1: Intramolecular Distances (in Å) and Bond Angles (in deg) of the NMA Monomer, Comparing ab Initio Calculations on the 3-21G Basis Set with Microwave and Electron Diffraction Gas-Phase Measurements

parameter	theory	expt[1]	expt[2]
CC	1.517	1.520	1.53
CO	1.219	1.224	1.21
CN	1.358	1.386	1.36
NH	0.996	(1.002)	
NC	1.461	1.468	1.44
(N)CH[a]	1.078	1.106	1.09
(N)CH[b]	1.084	1.106	1.09
(C)CH[a]	1.074	1.106	1.09
(C)CH[b]	1.084	1.106	1.09
∠CCN	114.0	114.1	113
∠OCN	123.0	121.8	125
∠CNH	119.6	110.0	107
∠CNC	121.8	119.6	117

[a] In-plane H atom. [b] Out-of-plane H atoms.

TABLE 2: Cooperative Energetics of H-Bonding in *N*-Methylacetamide Clusters, Showing the Calculated RHF/3-21G Energy (E_{RHF}, au), Counterpoise-Corrected Total Energy (E_{CP}, au), Average H-Bond Energy ($\Delta\bar{E}_{HB}$, kcal/mol), and Percentage Cooperative Enhancement (% coop., Relative to Dimer H-Bond Energy of 5.77 kcal/mol)

	species	E_{RHF} (au)	E_{CP} (au)	$\Delta\bar{E}_{HB}$, (kcal/mol)	% coop.
1.	NMA	−245.629 184			
2.	NMA2l	−491.276 255	−491.267 566	5.77	
3.	NMA3l	−736.927 947	−736.910 098	7.08	22.7
4.	NMA4l	−982.580 484	−982.553 134	7.61	31.9
5.	NMA5l	−1228.233 598	−1228.196 646	7.96	38.0

Because of computational limitations, clusters larger than pentamers were not possible. However, earlier calculations for formamide indicate that linear clusters larger than pentamers are highly unlikely.[63] The starting points for the ab initio calculations were linear NMA dimers, trimers, or tetramers. In the process of the energy minimization calculations, it was found that these linear oligomers do not form larger cyclic clusters, in contrast to the liquid state of formamide[63,64] and *N*-methylformamide.[65] In NMA the carbonyl proton is replaced by a methyl group, which sterically hinders the formation of cyclic clusters.

In the five structures considered, each interior monomer unit participates in a matched pair of H-bonds, once as a Lewis base (electron pair "donor") and once as a Lewis acid (electron pair "acceptor"). As described in previous studies of H-bond cooperativity, such bicoordinate structures allow intermolecular electron delocalization ("charge transfer") to occur in a maximally concerted manner, leading to strong enhancements of the binding energies. These cooperative effects lead to much stronger H-bond energies than are possible with only pairwise electrostatic interactions. For the linear trimer, tetramer, and pentamer species, where one, two, or three monomers participate as "donor" and "acceptor", the cooperative effects lead to H-bonding energies that are energetically 23, 32, and 38% stronger than the dimer hydrogen bond energy. The effectiveness of such topologies in increasing average H-bond strength is indicated in Table 2, where we present the calculated RHF/3-21G Hartree−Fock energy, the CP-corrected total energy (E_{CP}), the average binding energy per H-bond ($\Delta\bar{E}_{HB}$), and percentage cooperative enhancement (%-coop., with respect to

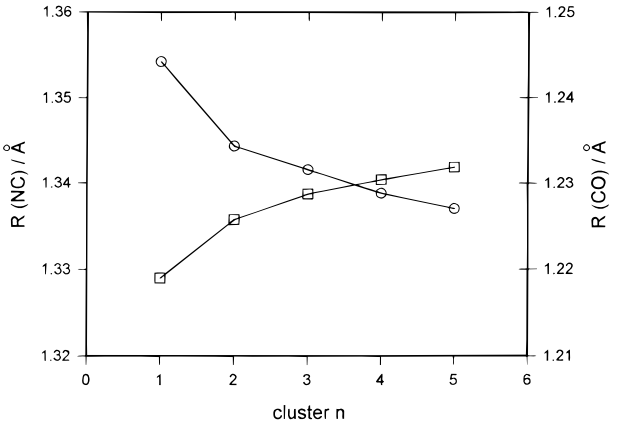

Figure 2. Ab initio calculated bond lengths r_{CN} (circles) and r_{CO} (squares) in NMA as a function of cluster size.

TABLE 3: Ab Initio Geometries (in Å) Calculated for Different Molecular Clusters of NMA. Average Values Are Shown in Parentheses

geometry	NMA	NMA2l	NMA3l	NMA4l	NMA5l
r_{NH}	0.9949	0.9948	0.9957	0.9958	0.9958
		1.0009	1.0032	1.0040	1.0043
			1.0031	1.0062	1.0071
				1.0039	1.0072
					1.0043
	(0.9949)	(0.9979)	(1.0007)	(1.0027)	(1.0037)
r_{CO}	1.2199	1.2278	1.2271	1.2276	1.2279
		1.2235	1.2325	1.2345	1.2352
			1.2246	1.2342	1.2363
				1.2251	1.2347
					1.2253
	(1.2199)	(1.2257)	(1.2281)	(1.2304)	(1.2319)
r_{CN}	1.3542	1.3421	1.3438	1.3332	1.3430
		1.3467	1.3354	1.3333	1.3326
			1.3456	1.3337	1.3315
				1.3451	1.3332
					1.3448
	(1.3542)	(1.3444)	(1.3416)	(1.3388)	(1.3370)
$r_{N\cdots O}$		2.9096	2.8753	2.8638	2.8595
			2.8719	2.8254	2.8129
				2.8608	2.8136
					2.8570
		(2.9096)	(2.8736)	(2.8500)	(2.8358)

H-bond strength in the *N*-methylacetamide dimer NMA2l) for all clusters. The cooperative energies cited here are "average" energies for complete dissociation to monomers. However, the actual H-bond energy to break a cluster into two subclusters is considerably larger than this "average" value and increases from the extremities toward the interior of the cluster. For the NMA linear pentamer, for example, the two possible H-bonds for dissociation to monomer + tetramer or dimer + trimer are 8.99 (55.8% cooperative) and 11.91 kcal/mol (106.4%), respectively.

This cooperative enhancement also leads to interesting geometries for the different NMA clusters. The 3-21G basis set at the Hartree−Fock level (which is readily applicable to such complex cluster species as *N*-methylacetamide) provides good geometries. As can be seen from Table 1, our calculated monomer geometries using the 3-21G basis set agree well with the experimental geometries of isolated gas-phase molecules obtained from microwave and electron diffraction studies.

The calculated geometries for all molecules in the clusters and the average geometries for the clusters are given in Table 3. In Figure 2 the variation of the r_{NC} and the r_{CO} bond lengths with cluster size is demonstrated. (Here, again, we are referring to average bond lengths. The bond lengths for the inner molecules change by a greater amount than those at the ends of the cluster.) As a consequence of cooperative enhancement,

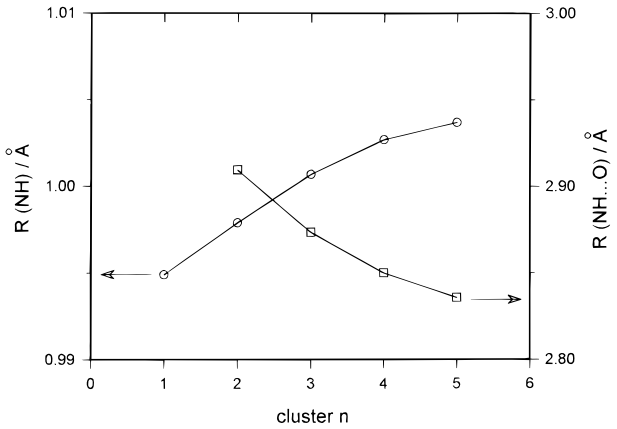

Figure 3. Ab initio calculated bond lengths r_{NH} (circles) and intermolecular peptide bond $r_{(O\cdots H-N)}$ (squares) of NMA clusters as a function of cluster size.

TABLE 4: Ab Initio Isotropic Chemical Shieldings (in ppm) of Oxygen, Nitrogen, and Amide Deuteron in Different Clusters of NMA (6-31G*). Average Values Are Shown in Parentheses

atom	NMA	NMA2l	NMA3l	NMA4l	NMA5l
O	−34.038	−13.059	−5.739	−3.288	−2.254
		−16.562	20.816	28.277	30.760
			−12.614	25.414	32.977
				−11.170	27.073
					−10.546
	(−34.038)	(−14.811)	(2.463)	(9.808)	(15.602)
N	184.167	182.898	181.904	181.562	181.414
		180.187	175.285	174.091	173.668
			179.299	174.089	172.821
				178.959	173.639
					178.818
	(184.167)	(181.543)	(178.829)	(177.175)	(176.072)
H	29.499	29.016	28.915	28.875	28.857
		26.080	25.394	25.200	25.125
			25.517	24.747	24.527
				25.354	24.556
					25.294
	(29.499)	(27.548)	(26.609)	(26.044)	(25.672)

r_{NC} decreases by about 1.7 pm and r_{CO} increases by about 1.2 pm going from the monomer up to the five-membered linear cluster values. A similar observation has been made by Otterson[30] comparing C−O and C−N bond lengths in solid and gaseous formamide and by Zeidler[71] comparing gas-phase geometries with the liquid structure of *N*-methylformamide.

The increasing hydrogen bond strength with larger cluster size lengthens the N−H bond by about 0.9 pm, as seen in Figure 3. It is also interesting to note the variation of the intermolecular peptide bond $r_{N\cdots O}$ shown in the same figure. The dimer value of about 291 pm decreases down to 284 pm in the linear pentamer of *N*-methylacetamide. This consequence of cooperativity was recently demonstrated by Saykally et al.,[72,73] who investigated experimentally the intermolecular distance $r_{O\cdots O}$ in different sized water clusters. As predicted by ab initio calculations, the $r_{O\cdots O}$ distance decreases with increasing cluster sizes.

The ab initio calculations of the isotropic chemical shieldings σ_H, σ_O, and σ_N of the amide proton, carbonyl oxygen, and nitrogen, respectively, for all nuclei and molecular clusters are given in Table 4. These σ values are the shifts with respect to the bare nucleus. Positive values indicate diamagnetic or lower frequency shifts; more negative values indicate paramagnetic or higher frequency shifts. (For an excellent discussion of the conventions used for chemical shifts and chemical shieldings, see ref 67.) The average values of the isotropic chemical shielding for each cluster are also listed in Table 4. The ^{1}H

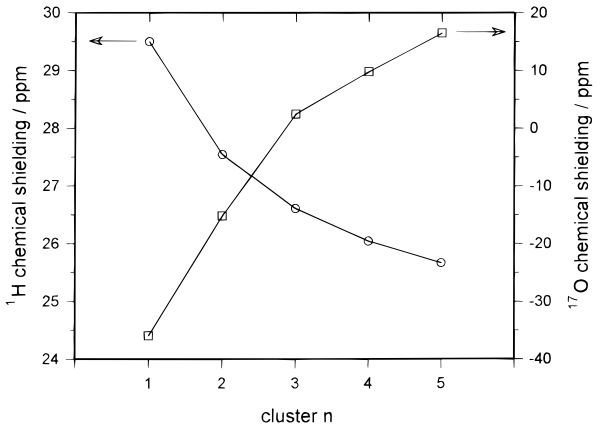

Figure 4. Ab initio calculated isotropic chemical shift values for the amide hydrogen (circles) and the carbonyl oxygen (squares) in different sized clusters ($n = 1-5$) of NMA.

TABLE 5: Ab Initio Quadrupole Coupling Constants (in MHz) of Oxygen, Nitrogen, and Amide Deuterons in NMA (6-31G*). Average Values Are Shown in Parentheses

atom	NMA	NMA2l	NMA3l	NMA4l	NMA5l
O	9.847	9.535	9.747	9.718	9.706
		9.857	9.290	9.195	9.164
			9.805	9.223	9.123
				9.790	9.200
					9.783
	(9.847)	(9.696)	(9.614)	(9.482)	(9.395)
N	4.030	3.862	3.985	3.972	3.966
		3.674	3.439	3.385	3.366
			3.605	3.352	3.294
				3.582	3.325
					3.573
	(4.030)	(3.768)	(3.676)	(3.573)	(3.5047)
D	0.2967	0.2953	0.2935	0.2932	0.2930
		0.2592	0.2519	0.2489	0.2479
			0.2511	0.2414	0.2386
				0.2484	0.2382
					0.2473
	(0.2967)	(0.2773)	(0.2655)	(0.2580)	(0.2530)

and ^{17}O chemical shieldings are shown in Figure 4. The ^{1}H chemical shielding moves to higher frequency by about 4 ppm whereas the ^{17}O chemical shielding shows a dramatic low-frequency shift of about 60 ppm going from the monomer to the linear pentamer.

The calculated QCC values and asymmetry parameters of the oxygen, nitrogen, and amide deuteron for all nuclei and clusters are given in Tables 5 and 6. The QCC values are determined by multiplying the main component, q_{zz} of the calculated efg tensor by the quadrupole moments of the oxygen (25.78 fm^2),[75] nitrogen (17.2 fm^2),[76] and deuteron (0.286 fm^2)[77] and a constant factor 2.3496, which takes care of the units. The average values of χ_Q and η_Q for each cluster are also listed in Tables 5 and 6. The values for χ_N and η_N for nitrogen are shown in Figure 5. The χ_N value decreases from 4.030 MHz for the monomer down to 3.505 MHz in the linear pentamer. The corresponding asymmetry parameters show the opposite behavior and increase from 0.0306 to 0.2773 in the same clusters. To the best of our knowledge, there are no experimental values available for χ_N or η_N for any of the nitrogen nuclei in NMA in either the gas phase or the solid state. With increasing cluster size the QCC values decrease and the asymmetry parameters increase relative to the gas-phase values. In previous studies of the quadrupole parameters of neat liquid water,[62] formamide,[63,64] and *N*-methylformamide,[65] we have shown theoretically that only large clusters showing strong cooperativity are in good agreement with the experimental values found in the liquid phase.

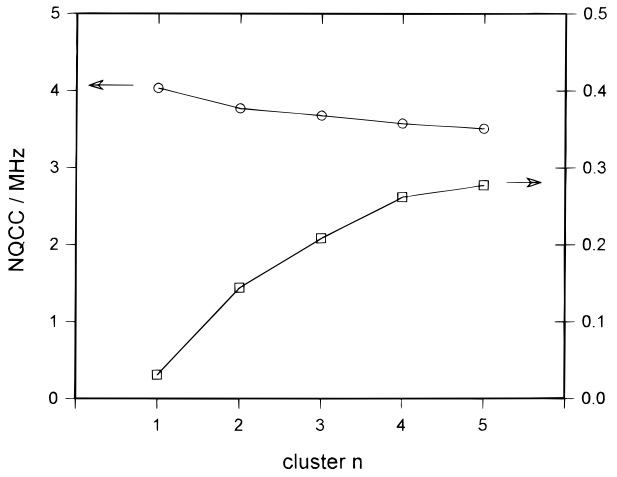

Figure 5. Ab initio calculated quadrupole coupling constants (circles) and asymmetry parameters (squares) for the nitrogen nuclei in different sized clusters ($n = 1-6$) of NMA.

TABLE 6: Ab Initio Asymmetry Parameters of Oxygen, Nitrogen, and Amide Deuterons, in NMA (6-31G*). Average Values Are Shown in Parentheses

atom	NMA	NMA2l	NMA3l	NMA4l	NMA5l
O	0.1943	0.3320	0.2971	0.3093	0.3145
		0.1962	0.4149	0.4583	0.4728
			0.2163	0.4392	0.4843
				0.2222	0.4477
					0.2250
	(0.1934)	(0.2641)	(0.3094)	(0.3573)	(0.3889)
N	0.0306	0.0416	0.0501	0.0509	0.0514
		0.2462	0.2874	0.3026	0.3087
			0.2865	0.3425	0.3611
				0.3000	0.3597
					0.3055
	(0.0306)	(0.1439)	(0.2080)	(0.2617)	(0.2773)
D	0.1982	0.1997	0.2012	0.2012	0.2012
		0.2283	0.2289	0.2295	0.2299
			0.2333	0.2360	0.2373
				0.2354	0.2386
					0.2361
	(0.1982)	(0.2140)	(0.2211)	(0.2255)	(0.2286)

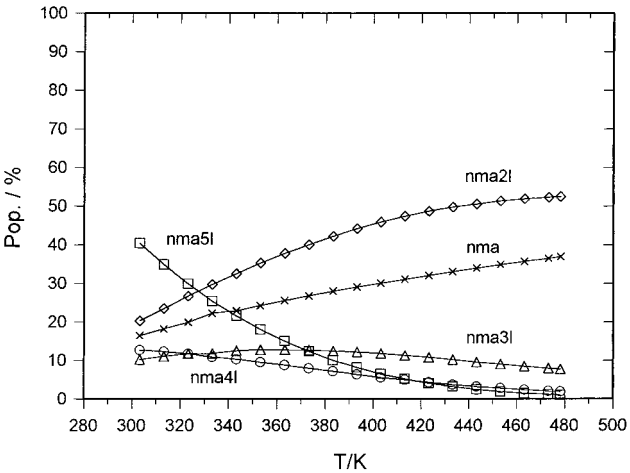

Figure 6. Cluster population for QCE(5)/3-21G model of NMA at $P = 1$ atm, showing the liquid−gas transition at 478.15 K.

4.2. QCE Population Distributions and Temperature-Dependent NMR Properties. The liquid-phase cluster populations obtained from thermodynamic calculations for temperatures in the range of 303 (melting point) to 478 K (boiling point) are listed in Table 7 and shown in Figure 6. Over the temperature range studied here the cluster populations change significantly. At low temperatures the linear pentamer is the

TABLE 7: Temperature-Dependent Percentage Population of NMA Clusters from Thermodynamic QCE/3-21G Calculations

T/K	NMA	NMA2l	NMA3l	NMA4l	NMA5l
303	16.5	20.3	10.2	12.7	40.4
313	18.2	23.5	11.1	12.3	34.9
323	19.9	26.7	11.7	11.7	29.9
333	22.3	29.7	11.8	10.9	25.4
343	22.9	32.6	12.6	10.3	21.6
353	24.3	35.3	12.8	9.6	18.1
363	25.6	37.8	12.8	8.8	15.1
373	26.8	40.1	12.7	8.0	12.4
383	28.0	42.2	12.5	7.2	10.1
393	29.1	44.2	12.2	6.4	8.2
403	30.1	45.9	11.8	5.6	6.5
413	31.1	47.4	11.3	5.0	5.2
423	32.1	48.7	10.8	4.3	4.1
433	33.1	49.8	10.2	3.7	3.2
443	34.0	50.6	9.6	3.2	2.5
453	34.9	51.4	9.1	2.8	1.9
463	35.7	51.9	8.5	2.4	1.5
473	36.5	52.3	8.0	2.1	1.2
478	36.9	52.5	7.7	1.9	1.0

dominant species. At higher temperatures the dominant species are monomer and dimer.

The calculated QCE values for the chemical shieldings and the QCC and asymmetry parameters for the amide proton/deuteron, carbonyl oxygen, and nitrogen in the liquid phase for NMA are obtained by weighting the macroscopic properties with the appropriate cluster populations. The values for the temperature range 303−478 K are given in Table 8. Since the temperature-dependent changes in the calculated populations are significant and the macroscopic properties for the oxygen, nitrogen, and trans deuteron are different for the different cluster species, the calculated chemical shielding, quadrupole coupling constants, and asymmetry parameters are expected to vary with temperature. This is, in fact, observed.

4.2.1. Comparison with Experimental NMR Shifts. To compare the theoretical shielding differences with experimental NMR shifts, we have chosen tetramethylsilane (TMS) and dimethyl sulfoxide (DMSO) as references for ^{1}H and ^{17}O, respectively. Unfortunately, the isotropic shieldings for both references change slightly with temperature. Their temperature dependence is about 10% of the ^{1}H and ^{17}O shifts for NMA. Instead of using the relative shifts between the reference and NMA over the whole temperature range, we determined the differences only for the reference value at its lowest temperature, 303 K. Thus for all higher temperatures we performed the experiment at constant magnetic field (without an internal lock) measuring the ^{17}O and ^{1}H chemical shift values relative to the reference value at 303 K. The theoretical chemical shifts were obtained by subtracting the population weighted average chemical shieldings values for NMA from the calculated chemical shielding values for the references. The chemical shielding values for the references were 32.86 ppm for ^{1}H in TMS and 356 ppm for ^{17}O in DMSO.[74] For nitrogen no internal reference was used because the chemical shifts for all available reference compounds depend strongly on temperature and solvent. Here the nitrogen experimental chemical shift and the theoretical chemical shielding value were set to zero at 313 K, and the relative shifts were determined as a function of temperature.

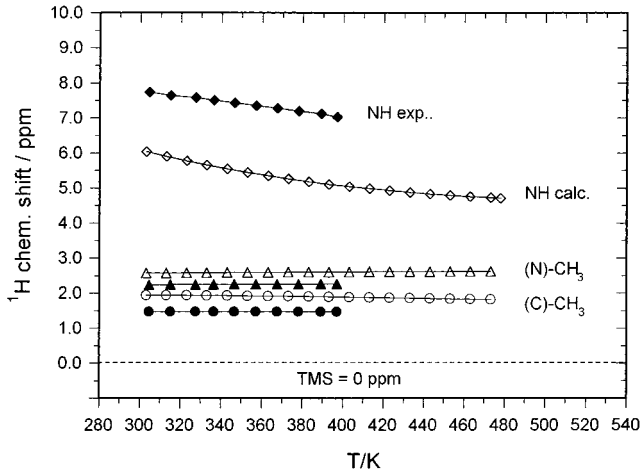

Figure 7. Calculated (open diamonds) and experimental (filled diamonds) isotropic chemical shift values for the amide proton in liquid *N*-methylacetamide as a function of temperature. For comparison the chemical shifts for both methyl groups are shown. All experimental (filled symbols) and theoretical data (open symbols) are plotted versus TMS.

In Figures 7, 8, and 9 we show a comparison of the temperature dependence of the calculated proton, oxygen, and nitrogen chemical shift values with the observed values. The theoretical and experimental temperature dependencies are in almost quantitative agreement. For the temperature range 303−

TABLE 8: Calculated Chemical Shieldings (in ppm), Quadrupole Coupling Constants (in MHz), and Asymmetry Parameters for the Amide Deuteron, the Nitrogen, and Oxygen in Liquid NMA

	O			N			D		
T (K)	σ (ppm)	χ_Q (MHz)	η_Q	σ (ppm)	χ_Q (MHz)	η_Q	σ (ppm)	χ_Q (MHz)	η_Q
303	26.823	0.2670	0.2194	178.93	3.670	0.2007	−0.7787	9.563	0.3194
313	26.956	0.2686	0.2184	179.27	3.689	0.1948	−2.7406	9.583	0.3113
323	27.087	0.2702	0.2174	179.59	3.707	0.1827	−4.593	9.601	0.3037
333	27.206	0.2716	0.2164	179.89	3.724	0.1746	−6.322	9.617	0.2967
343	27.317	0.2730	0.2156	180.17	3.739	0.1670	−7.931	9.633	0.2902
353	27.417	0.2742	0.2148	180.42	3.753	0.1600	−9.399	9.647	0.2843
363	27.511	0.2754	0.2141	180.66	3.766	0.1536	−10.761	9.660	0.2788
373	27.598	0.2764	0.2134	180.87	3.778	0.1477	−12.015	9.671	0.2739
383	27.677	0.2775	0.2128	181.07	3.789	0.1423	−13.166	9.682	0.2694
393	27.750	0.2782	0.2122	181.25	3.799	0.1373	−14.221	9.691	0.2653
403	27.817	0.2790	0.2117	181.41	3.807	0.1327	−15.177	9.700	0.2616
413	27.877	0.2797	0.2112	181.55	3.815	0.1287	−16.034	9.707	0.2583
423	27.931	0.2804	0.2108	181.68	3.823	0.1250	−16.812	9.714	0.2554
433	27.980	0.2810	0.2104	181.79	3.829	0.1217	−17.503	9.720	0.2528
443	28.024	0.2815	0.2101	181.89	3.845	0.1187	−18.117	9.715	0.2506
453	28.064	0.2819	0.2097	181.98	3.840	0.1161	−18.661	9.729	0.2486
463	28.099	0.2823	0.2095	182.06	3.845	0.1137	−19.147	9.733	0.2469
473	28.131	0.2827	0.2092	182.13	3.849	0.1117	−19.579	9.736	0.2453
478	28.146	0.2829	0.2090	182.16	3.851	0.1107	−19.779	9.738	0.2446

393 K, the calculated ^{1}H chemical shift of the amide proton moves to higher frequency by 0.93 ppm, compared to 0.71 ppm in the NMR experiment. With increasing temperature, hydrogen bonds are broken, the amide proton becomes more shielded, and the resonance moves toward the TMS signal. For comparison, the proton chemical shifts for both methyl groups of NMA are also shown in Figure 7. Both theory and experiment show that the methyl chemical shifts are essentially temperature-independent. This is expected because, in contrast to the amide proton, the methyl protons are not involved in hydrogen bonding. Consequently, no temperature dependence is observed.

The calculated ^{17}O chemical shift values change by about 12.4 ppm to lower frequency compared with the experimental change of 11.1 ppm. The calculated absolute value for ^{17}O shift at a given temperature differs from the experimental value by about 60 ppm. This poor agreement is due to the difficulty in calculating the oxygen chemical shielding. Similarly, the calculated ^{17}O chemical shift values for the DMSO reference and the experimental values differ by about 30 ppm. Here again, however, the temperature-dependent behavior is reproduced nearly quantitatively. The observed nitrogen chemical shift changes by 2.32 ppm over the temperature range, in excellent agreement with the theoretically predicted change of 2.26 ppm. As with the temperature dependence of the proton chemical shift, this change is primarily due to the fact that with increasing temperature the N−H bond distance increases and the C−N bond distance decreases. Although some of the temperature-dependent changes are very small (1 ppm) and others are quite large (up to 12 ppm), all of the changes were accurately predicted by using the population weighted properties resulting from the QCE model and ab initio calculations.

4.2.2. Comparison with Experimental QCC and Asymmetry Parameters. For the nitrogen, oxygen, and the amide deuteron, theory predicts temperature-dependent changes for the QCC values of up to 5% with temperature. The calculated oxygen QCC value increased from 9.56 MHz at 303 K to 9.74 MHz at 378 K, the boiling point of *N*-methylacetamide. This temperature behavior is expected since the oxygen nuclei are involved in hydrogen bonding with the amide deuteron. Increasing temperature leads to hydrogen bond breaking and a consequent rise in the value of the QCC toward the gas-phase value.

It is interesting to note that the oxygen asymmetry parameter for NMA decreases with increasing temperature. Although no experimental data are available for NMA asymmetry parameters, the values and the trends in the values should be similar to those for NMF. The liquid *N*-methylformamide asymmetry parameter value of 0.319 for η_O at 303 K is below the solid-phase value of 0.45.[78] This liquid-state value decreases with increasing temperature to a value of 0.245 at the boiling point. In a similar fashion, theory predicts that as the temperature of neat, liquid NMF increases from 303 to 478 K, the nitrogen and the amide deuteron QCC values will increase from 3.67 to 3.85 MHz and from 267.0 to 282.9 kHz, respectively. The corresponding asymmetry parameters drop from 0.201 to 0.112 and from 0.219 to 0.209.

Values for quadrupole coupling constants for molecules in the gas phase are available from microwave spectroscopy, and those for the solid phase can be measured by nuclear quadrupole or magnetic resonance. For nitrogen and the amide deuteron in the liquid state, experimental QCC data are available indirectly from NMR relaxation time experiments.[79] A comparison of theoretical and experimental liquid values requires an understanding of how such NMR measurements are made.

The general expression for the longitudinal relaxation rate arising from the quadrupole interaction, $R_1(Q)$, is given by[80]

$$\left(\frac{1}{T_1}\right)_Q = \mathrm{R}_1(Q) = \frac{3}{10}\pi^2\frac{2I+3}{I^2(2I-1)}\left(1+\frac{\eta_Q^{\,2}}{3}\right)\left(\frac{\mathrm{e}Q\,eq}{h}\right)_Q^{\,2}\tau_c$$

$$= \frac{3}{10}\pi^2\frac{2I+3}{I^2(2I-1)}\left(1+\frac{\eta_Q^{\,2}}{3}\right)\chi_Q{}^2\tau_c$$

$$= \frac{3}{10}\pi^2\frac{2I+3}{I^2(2I-1)}\chi_Q{}^2(\mathrm{eff})\tau_c \qquad (1)$$

where eQ is the nuclear quadrupole moment, eq is the principal axis component of the electric field gradient tensor, η_Q is the asymmetry parameter for the electric field gradient tensor, I is the nuclear spin quantum number ($I = 1$ for ^{2}H and ^{14}N), h is Planck's constant, and

$$\chi_Q = eQ\,eq/h$$

is the quadrupole coupling constant in units of s^{-1}; the above expression holds only in the extreme narrowing region (where $\omega_0\tau_c \ll 1$). If the correlation time τ_c is known, then a measurement of the relaxation rate, R_1, provides a value χ_Q(eff). In the NMR experiment a separate determination of the QCP value and the asymmetry parameter is not possible for the liquid phase.

The molecular correlation time, τ_c, can be obtained from dipolar relaxation time experiments if the coupling parameter, the bond distance for the two dipolar nuclei, is known from diffraction experiments in the liquid phase.[71] Seipelt[79] determined the amide deuteron and the nitrogen-14 QCC values for neat, liquid NMA for temperatures between 300 and 378 K. Her experimental data are shown in Figures 10 (D) and 11 (^{14}N) along with the calculated QCC values from Table 6. Both the experimental and the theoretical QCC values show the same trend with temperature, but with appreciable quantitative differences. Over the entire temperature range, the amide deuteron QCC value increases by about 3 kHz experimentally; the calculations predict an increase of 10 kHz. Similarly, the experimental nitrogen-14 QCC value increases by about 0.35 MHz and the theoretical value increases by 0.12 MHz.

Although the experimentally observed temperature behavior for both nitrogen and deuterium is in tolerable agreement with the theoretical predictions, there are large differences in the absolute values (up to 40% for the nitrogen). The discrepancies in the absolute values most probably arise from systematic experimental errors. Different techniques and evaluation procedures were used to determine the rotational correlation times that were used to calculate the QCC values. For liquid formamide the molecular motions are isotropic. In this case knowledge of the C−H bond distance and a measurement of the carbon-13 relaxation rate provide an accurate value for the molecular correlation time and the correlation time of the principal axes of the oxygen, nitrogen, and deuterium efg tensors. The molecular motions in NMA are not isotropic. To obtain values for the correlation time of the N−H internuclear vector and the principal axis of the deuterium efg tensor, the amide proton relaxation time was measured for a sample of normal (^{14}N) NMA and for nitrogen-15-labeled NMA. The difference between the rates in the normal and labeled samples provides information about the intramolecular proton relaxation arising from the nitrogen to which it is bonded.

Since the magnetic moments of nitrogen-14 and nitrogen-15 are of comparable magnitude, the difference in these two rates

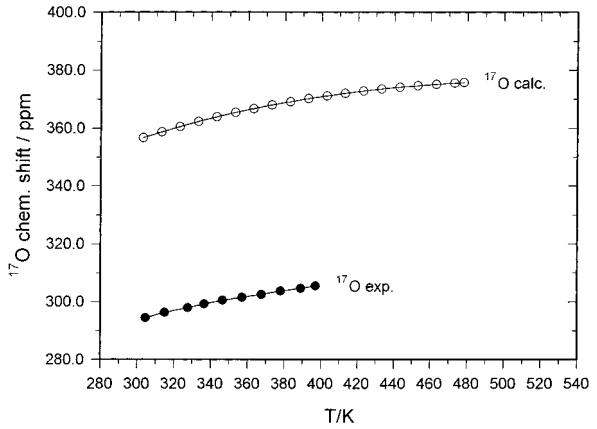

Figure 8. Calculated (open circles) and experimental (filled circles) isotropic chemical shift values for the carbonyl oxygen in liquid *N*-methylacetamide as a function of temperature. All data are plotted versus DMSO.

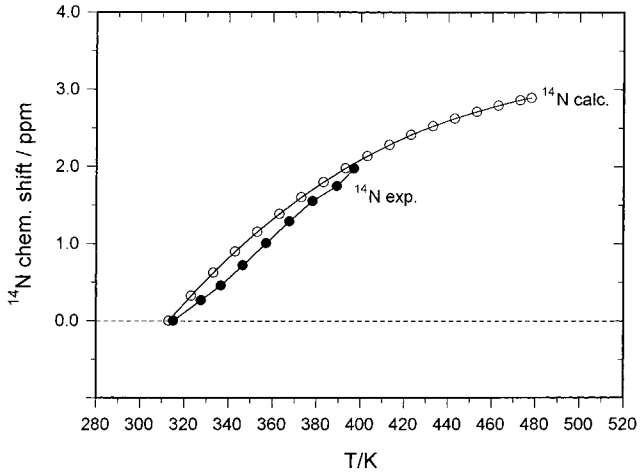

Figure 9. Calculated (open circles) and experimental (filled circles) isotropic chemical shift values for the nitrogen in liquid *N*-methylacetamide as a function of temperature.

TABLE 9: Comparison of the Population-Weighted Geometries Obtained from the QCE/3-21G Model for Liquid NMA at 303 K and from X-ray Diffraction Data in the Solid

	theory	X-ray[3]	X-ray[4]
CC	1.518	1.536	1.515
CO	1.228	1.236	1.246
CN	1.342	1.290	1.325
NH	1.001		
NC	1.460	1.465	1.454
NH···O	2.863	2.825	

is relatively small. In addition, the other contributions to the amide proton relaxation are comparable to the contribution from the intramolecular N−H dipolar contribution. The result is that the uncertainties in the measurement of the correlation time for the N−H internuclear vector (or the deuterium efg tensor component) are rather large. For this reason it is not surprising that the agreement between the experimental and theoretical results is substantially poorer than was the case for our study of neat, liquid formamide. Within the limits of experimental error, the experimental QCC values and the theoretically calculated ones show the same trend with temperature; increasing temperature leads to hydrogen bond breaking and to a rise in the QCC values.

4.3. Comparison with Experimental Geometry Measures. Equilibrium molecular geometries can be calculated for liquid NMA. Unfortunately, there are no geometries available from diffraction experiments for the liquid phase. Therefore, we use

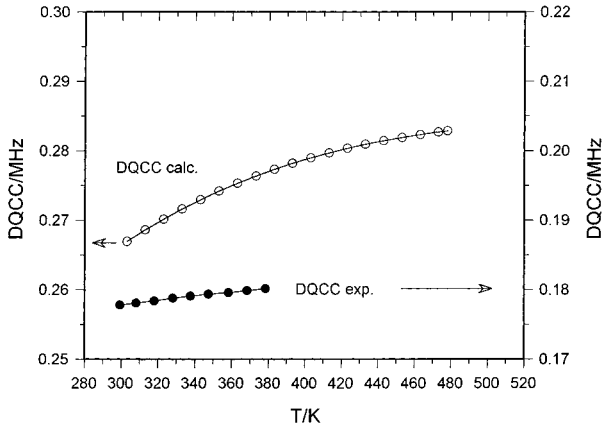

Figure 10. Temperature-dependent calculated (open circles) and experimental (filled circles)[79] QCC values for the amide deuteron in liquid *N*-methylacetamide.

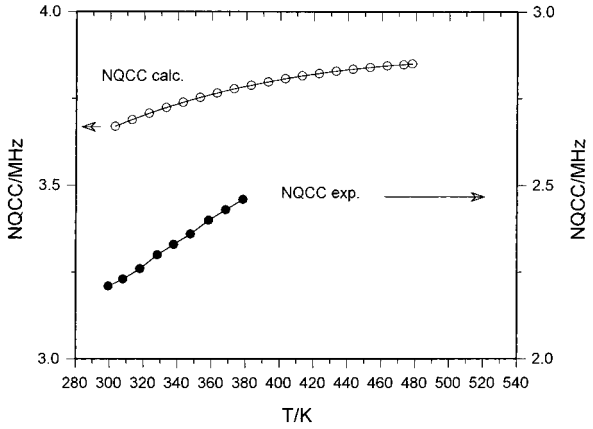

Figure 11. Temperature-dependent calculated (open circles) and experimental (filled circles)[79] QCC values for the nitrogen nuclei in liquid *N*-methylacetamide.

intra- and intermolecular geometries obtained from the QCE model and Gaussian-94 calculations at 303 K and compare them with available structure data from X-ray measurements in solid NMA.[3,4] The results are shown in Table 9. The geometries in both phases show the typical behavior of hydrogen-bonded systems. The C═O bond becomes shorter and the C−N bond becomes longer in the transition from the solid phase to the liquid phase. Since the methyl groups are not involved in hydrogen bonding, no geometrical changes are expected with the phase transition. This expectation is confirmed by both the experimental data and the ab initio calculations.

We are especially interested in the temperature dependence of the intermolecular $r_{O\cdots H-N}$ peptide bond. Our calculated temperature-dependent values of this bond length are shown in Figure 12. All data show a longer $r_{O\cdots HN}$ bond length than the experimental X-ray value of 282.5 pm for solid NMA. The calculations predict that the peptide bond increases from 286 pm at 303 K to 290 pm at 378 K. This temperature-dependent change of about 4 pm is within the range of current experimental uncertainty. For the similar molecule NMF one observes an $r_{O\cdots N-H}$ H-bond distance of 273 pm (172 pm for $r_{O\cdots N}$ and 100.7 pm for r_{NH}) from neutron diffraction[71] and about 298 pm from X-ray diffraction studies.[81] An accurate temperature-dependent neutron diffraction measurement of the peptide hydrogen bond in NMA is clearly needed to make a careful test of the QCE model and its ability to predict accurately the temperature-dependent behavior of the cluster.

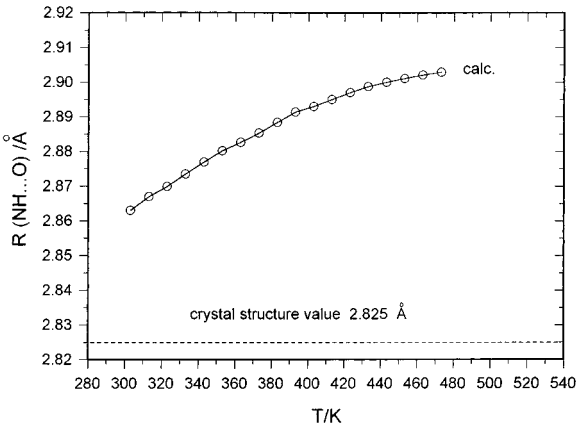

Figure 12. Intermolecular peptide bond $r_{(O\cdots H-N)}$ of liquid *N*-methylformamide as a function of temperature. For comparison the X-ray value obtained for solid NMA is shown.[3]

5. Conclusions

The foregoing results provide a stringent and comprehensive experimental test of the ab initio QCE/3-21G model of liquid *N*-methylacetamide, based on a wide variety of structural, NMR, and quadrupole coupling measurements and their temperature dependence over the entire liquid range. Despite the relatively large uncertainties (primarily of experimental origin) associated with some of these comparisons, one can conclude that *all available* experimental measurements are in reasonable qualitative or near quantitative agreement with the theoretical QCE model. In view of the simplicity of the current QCE model, and the many possibilities for its improvement, the current agreement between theory and experiment is considered satisfactory.

We have pointed out where further measurements could be extremely useful in testing the QCE model of the liquid structure. These include temperature-dependent neutron diffraction or X-ray studies to check the predicted geometry changes with temperature. Pressure-dependent experiments for all hydrogen-bonding properties are also highly desirable to check whether the QCE model is able to reproduce pressure dependence as well as temperature-dependent changes in molecular and electronic structure.

Combined with previous results for water, formamide, and *N*-methylformamide (and with an experimental infrared study which is in progress), our results suggest that the QCE methodology can be applied successfully to a wide range of hydrogen-bonded liquids with markedly different clustering patterns. Current studies in this laboratory are devoted to a much broader spectrum of H-bonded liquids, including binary solutions, that will further test the limits of the QCE approach.

Acknowledgment. We thank the National Science Foundation, Grant CHE-9500735, for the support of this research. One of the authors (R.L.) thanks the Deutsche Forschungsgemeinschaft and the Fonds der Chemischen Industrie for financial support. We thank Mark Wendt for help with some of the drawings.

References and Notes

(1) Kitano, M.; Fukuyama, T.; Kuchitsu, K. *Bull. Chem. Soc. Jpn.* **1973**, *46*, 384.
(2) Kimuara, M.; Aoki, M. *Bull. Chem. Soc. Jpn.* **1953**, *26*, 429.
(3) Katz, J. L.; Post, P. *Acta Crystallogr.* **1960**, *13*, 624.
(4) Hamazaoui, F.; Baert, F. *Acta Crystallogr.* **1994**, *C50*, 757.
(5) Itoh, K.; Shimanouchi, T. *Bioploymers* **1967**, *5*, 921.
(6) Fillaux, F.; Baron, M. H. *Chem. Phys.* **1981**, *62*, 275.
(7) Fillaux, F.; De Loze, C. *Chem. Phys. Lett.* **1976**, *36*, 547.
(8) Polavarapu, P. L.; Deng, Z.; Ewig, C. S. *J. Phys. Chem.* **1994**, *98*, 9819.
(9) Kuznetsova, L. M.; Furer, V. L.; Maklakov, L. I. *J. Mol. Struct.* **1996**, *380*, 23.
(10) Gellman, S. H.; Dado, G. P.; Liang, G. B.; Adams, B. R. *J. Am. Chem. Soc.* **1991**, *113*, 1164.
(11) Mayne, L. C.; Ziegler, L. D.; Hudson, B. *J. Chem. Phys.* **1985**, *89*, 3395.
(12) Nielson, O. F.; Christensen, D. H.; Rasmussen, O. H. *J. Mol. Struct.* **1991**, *242*, 273.
(13) Wang, Y.; Purcello, R.; Georghiou, S.; Spiro, T. G. *J. Am. Chem. Soc.* **1991**, *113*, 6368. 6359.
(14) Triggs, N. E.; Valetini, J. J. *J. Phys. Chem.* **1992**, *96*, 6922.
(15) Didik, J. M.; Johnson, C. R.; Asher, S. A. *J. Phys. Chem.* **1985**, *89*, 3805.
(16) Harada, I.; Sugawara, Y.; Matsuara, H.; Shimanouchi, T. *J. Raman Spectrosc.* **1975**, *4*, 91.
(17) Song, S.; Asher, S. A.; Krimm, S.; Bandekar, J. *J. Am. Chem. Soc.* **1988**, *110*, 8547.
(18) Song, S.; Asher, S. A.; Shaw, K. D. *J. Am. Chem. Soc.* **1991**, *113*, 1155.
(19) Chen, X. G.; Asher, S. A.; Schweitzer-Stenner, R.; Mirkin, N. G.; Krimm, S. J. *J. Am. Chem. Soc.* **1995**, *117*, 2884.
(20) Mayne, L. C.; Hudson, B. S. *J. Phys. Chem.* **1991**, *95*, 2962.
(21) Burgar, M.; St. Amour, T. E.; Fiat, D. *J. Chem. Phys.* **1981**, *85*, 502.
(22) Gerothanassis, I.; Vakka, C. *J. Org. Chem.* **1994**, *59*, 2341.
(23) Glushka, J.; Lee, M.; Coffin, S.; Cowburn, D. *J. Am. Chem. Soc.* **1989**, *111*, 7716.
(24) Akiyama, M.; Othani, T. *Spectrochimica Acta*, **1994**, *50*, 317.
(25) Pralat, K.; Jadzyn, J.; Balanicka, S. *J. Phys. Chem.* **1983**, *87*, 1385.
(26) Omar, M. M. *J. Chem. Soc., Faraday Trans. 1* **1978**, *74*, 115.
(27) Mirkin, N. G.; Krimm, S. *J. Mol. Struct.* **1991**, *242*, 143.
(28) Sugawara, Y.; Hirakawa, A. Y.; Tsuboi, M. *J. Mol. Struct.* **1984**, *108*, 206.
(29) Sugawara, Y.; Hirakawa, A. Y.; Tsubori, M.; Kato, S.; Morokuma, M. *J. Mol. Spectrosc.* **1986**, *115*, 21.
(30) Otterson, T. *Adv. Mol. Relax. Processes* **1976**, *9*, 105.
(31) Jorgensen, W. L.; Gao, J. L. *J. Am. Chem. Soc.* **1988**, *110*, 4212.
(32) Cheam, T. C.; Krimm, S. *J. Mol. Struct.* **1986**, *146*, 178.
(33) Forgarasi, G.; Pulay, P.; Torok, J. *Mol. Struct.* **1979**, *57*, 259.
(34) Balazs, A. *J. Mol. Struct.* **1979**, *57*, 259.
(35) Yu, H. A.; Karplus, M.; Petitt, B. M. *J. Am. Chem. Soc.* **1991**, *113*, 2435.
(36) Williams, R. W. *Biopolymers* **1992**, *32*, 829.
(37) Cheam, T. C. *J. Mol. Struct.* **1992**, *257*, 57.
(38) Guo, H.; Karplus, M. *J. Phys. Chem.* **1992**, *96*, 7273.
(39) Guo, H.; Karplus, M. *J. Phys. Chem.* **1994**, *98*, 7104.
(40) Luque, F. J.; Orozco, M. *J. Org. Chem.* **1993**, *58*, 6397.
(41) Cieplak, P.; Kollmann, P. *J. Comput. Chem.* **1991**, *12*, 1232.
(42) Radom, L.; Riggs, N. V. *Aust. J. Chem.* **1982**, *35*, 1071.
(43) Mirkin, N. G.; Krimm, S. *J. Am. Chem. Soc.* **1991**, *113*, 9742.
(44) Ataka, S.; Takeuchi, H.; Tasumi, M. *J. Mol. Struct.* **1984**, *113*, 147.
(45) 'Radzicka, A.; Pedersen, L.; Wolfenden, R. *Biochemistry* **1988**, *27*, 4538.
(46) Barker, R. H.; Bourdreaux, G. J. *Spectrochim. Acta* **1967**, *23A*, 727.
(47) Jeffrey, G. A.; Saenger, W. *Hydrogen Bonding in Biological Structures*; Springer-Verlag; Berlin, 1991.
(48) Stickle, D. F.; Presta, L. G.; Rose, K. A. *J. Mol. Biol.* **1992**, *226*, 1143.
(49) Kauzmann, W. *Adv. Protein Chem.* **1959**, *14*, 1.
(50) Tanford, C. *Adv. Protein Chem.* **1968**, *23*, 121.
(51) Singer, S. J. *Adv. Protein Chem.* **1961**, *17*, 1.
(52) Nelson, J. W.; Kallenbach, N. R. *Proteins* **1986**, *1*, 211.
(53) Storrs, R. W.; Truckses, D.; Wemmer, D. E. *Biopolymers* **1992**, *32*, 1695.
(54) Sonnichsen, F. D.; Van Eyk, J. E.; Hodges, R. S.; Sykes, B. D. *Biochemistry* **1992**, *31*, 8790.
(55) Brooks, B. R.; Bruccoleri, R. E.; Olafson, B. D.; States, D. J.; Swaminthan, S.; Karplus, M. *J. Comput. Chem.* **1983**, *4*, 187.
(56) Deslaurier, R.; Smith, I. C. P. *Biol. Magn. Reson.* **1980**, *2*, 243.
(57) Soda, G.; Chiba, T. *J. Phys. Soc. Jpn.* **1969**, *26*, 249.
(58) Soda, G.; Chiba, T. *J. Chem. Phys.* **1969**, *50*, 439.
(59) Berglund, B.; Lindgren, J.; Tegenfeldt, T. *J. Mol. Struct.* **1978**, *43*, 179.
(60) Weinhold, F. *J. Mol. Struct. (THEOCHEM)* **1997**, *398*, 181.
(61) Hirschfelder, J. O.; Curtiss, C. F.; Bird, B. R. *Molecular Theory of Gases and Liquids*; Wiley: New York, 1954; p 28.
(62) Ludwig, R.; Weinhold, F.; Farrar, T. C. *J. Chem. Phys.* **1995**, *103*, 6941.
(63) Ludwig, R.; Weinhold, F.; Farrar, T. C. *J. Chem. Phys.* **1995**, *102*, 5118.

(64) Ludwig, R.; Weinhold, F.; Farrar, T. C. *J. Chem. Phys.* **1995**, *103*, 3636.

(65) Ludwig, R.; Weinhold, F.; Farrar, T. C. *J. Chem. Phys.*, submitted.

(66) To be published.

(67) Duncan, T. M. *A Compilation of Chemical Shift Anisotropies*; The Farragut Press; Madison, 1990.

(68) Boys, S. F.; Bernardi, F. *Mol. Phys.* **1970**, *19*, 553.

(69) For an authorative description of the ab initio methods and basis sets employed here: Hehre, W. G.; Radom, L.; Schleyer, P. v. R.; Pople, J. A. *Ab Initio Molecular Orbital Theory*; Wiley: New York, 1986.

(70) G94: Frisch, M. J.; Trucks, G. W.; Schlegel, H. B.; Gill, P. M. W.; Johnson, B. G.; Robb, M. A.; Cheeseman, J. R.; Keith, T. A.; Peterson, G. A.; Montgomery, J. A.; Raghavachari, K.; Laham, M. A.; Zakrzewski, V. G.; Ortiz, J. V.; Foresman, J. B.; Cioslowski, J.; Stefanov, B.; Nanayakkara, A.; Challacombe, M.; Peng, C. Y.; Ayala, P. Y.; Chen, W.; Wong, M. W.; Andres, J. L.; Replogle, E. S.; Gomperts, R.; Martin, R. L.; Fox, D. J.; Binkley, J. S.; Defrees, D. J.; Baker, J.; Steward, J. J. P.; Head-Gordon, M.; Gonzalez, C.; Pople, J. A. *Gaussian 94 (Revision A.1)*; Gaussian, Inc.: Pittsburgh, PA, 1995.

(71) Neuefeind, J.; Chieux, P.; Zeidler, M. D. *Mol. Phys.* **1992**, *676*, 143.

(72) Cruzan, J. D.; Braly, L. B.; Liu, K.; Brown, M. G.; Loeser, J. G.; Saykally, R. J. *Science* **1996**, *271*, 59.

(73) Liu, K.; Brown, M. G.; Cruzan, J. D.; Saykally, R. J. *Science* **1996**, *271*, 62.

(74) Kutzelnigg, W.; Fleischer, U.; Schindler, M. The IGLO Method: *Ab initio* Calculation; Interpretation of NMR Chemical Shifts and magnetic Susceptibilities. In *NMR Basis Principles and Progress*; Diehl, P., Fluck, E., Günther, H., Kosfeld, R., Seelig, J., Eds.; Springer-Verlag: New York, 1991, Vol. 23.

(75) Boykin, D. W. In ^{17}*O NMR Spectroscopy in Organic Chemistry*; CRC Press: Boca Raton, 1990.

(76) Palmer, M. H. *Chem. Phys.* **1988**, *127*, 335.

(77) Huber, H. *J. Chem. Phys.* **1985**, *83*, 4591.

(78) Chang, C. P.; Brown, T. L. *J. Am. Chem. Soc.* **1979**, *101*, 2327.

(79) Seipelt, C. Dissertation, RWTH Aachen, 1996.

(80) Abragam, A. *Principles of Nuclear Magnetism*; Oxford University Press: London, 1961.

(81) Ohtaki, H.; Itoh, S.; Rohde, B. M. *Bull. Chem. Soc. Jpn.* **1986**, *59*, 271.